

New Folder Name Test Mass Suspension

and Control Concept

Test Mass Suspension and Control Concept for Initial LIGO Receivers

S. Kawamura L. Sievers M. E. Zucker

Draft 3.0, 27 September 1991; rev. A, 10 April 1992

Abstract

We present a simple conceptual design for an interferometer test mass suspension and control subsystem and evaluate its consistency with the mission of initial LIGO receivers. Theoretically calculable noise mechanisms, risks, and scalability from onhand laboratory experience are discussed.

LIGO WORKING DOCUMENT
ALL DATA ARE PRELIMINARY

DO NOT DISTRIBUTE WITHOUT AUTHORIZATION

Contents

1 Introduction	4
1.1 Scope	4
1.2 Goals and design strategy	4
2 Base design summary	4
2.1 Test mass	4
2.2 Suspension	5
2.3 Sensors and actuators	6
2.4 Control systems	7
3 Departures from direct prototype scaling	8
3.1 Monolithic mirror/mass	8
3.2 Single loop suspension	8
3.3 Reference/mounting for sensors and actuators	8
3.4 Direct magnetic drive for all degrees of freedom	10
3.5 Low bandwidth damping and control loops	10
4 Risks and open questions	10
4.1 Thermal noise	10
4.1.1 Internal test mass modes	10
4.1.2 Pendulum mode	11
4.1.3 Vertical wire extension mode	11
4.2 Magnet-related noise	11
4.2.1 Lightning storms	11
4.2.2 Barkhausen effect	11
4.2.3 Glue joint noise	12
4.2.4 Eddy current Q degradation or seismic “short”	12
4.3 Control system driver output noise	12
A Alternate suspension arrangements	13
A.1 Double pendulum	13
A.2 Multiwire single pendulum	13
B Control system sensor noise	14
B.1 Coupling to transverse or vertical damping	14
B.2 Coupling to optical lever noise	15
C Optical lever concept and noise estimate	17
D Direct magnetic drive noise calculations	18
D.1 Peak force and required magnet size	18
D.2 Coupling of seismic noise through force gradients	20
D.3 Pendulum Q limits and thermal noise	21
D.4 Noise from glue joints	22

D.5	Magnetization fluctuation	23
D.6	Environmental magnetic interference	24
D.6.1	Broadband A.C. fields and gradients	24
D.6.2	Local currents in the laboratory	25
D.6.3	Lightning events	26

List of Figures

1	Test mass schematic diagram	5
2	Suspension cage concept	6
3	Control system topology	9
4	Local damping control loop transfer function	9
5	Control system noise	16
6	OSEM force vs. distance	20

1 Introduction

1.1 Scope

The test mass suspension and control subsystem [1] comprises the test mass itself as well as mechanical hardware, sensors and actuators, and control system electronics which suspend the test mass from the Seismic Isolation Stack subsystem and damp and control its degrees of freedom. Some important interfaces to other receiver systems are as follows:

- *mechanical*; the subsystem is fixed to the terminating surface of the Seismic Isolation Stack subsystem.
- *optical*; the mirror coating and substrate optical properties will be dictated by optical requirements of the Cavity and Interferometer systems.
- *external control inputs*; provision is made for introducing corrective and calibration forces (originated by Interferometer and Calibration systems) and torques (originated by the Alignment system).
- *vacuum*; the construction is consistent with pressure and pump speed specs in the test mass chambers

1.2 Goals and design strategy

The selection of a baseline design has followed the general principle of directly copying and/or scaling analogous systems and structures from the prototype instruments (principally the 40m prototype) and evaluating their scaled performance characteristics. Departures from tested designs are adopted only if forced by a clear conflict with performance goals of the Initial Receiver. Some of these goals are summarized in Figure V-3 and Table V-2 of the construction proposal [10, pages 48-51], which address target strain sensitivity. It should be emphasized that other goals, including interferometer duty cycle, veto capability for interfering signals, and an absolute bare minimum R&D path to final engineering design and construction are also highly important.

We begin by summarizing features and parameters of the base design concept. Options, risks and decisions encountered in arriving at this concept are discussed later sections. §3 documents significant departures from the existing prototype design. §4 summarizes some important risk factors to be addressed by future experimental and theoretical work. Noise models relevant to the performance and suitability of the design are developed in the Appendices.

2 Base design summary

2.1 Test mass

The test mass is a right circular cylinder of fused silica. It has a diameter of 20cm and a mass of 10kg, making the thickness approximately 16cm. A small wedge angle

(TBD) is included between the faces to discourage optical interference. The test mass is superpolished and optically coated on both faces (we will refer to the *front* as the reflective face and the *back* as the AR coated face) and has an industrial-grade polish on the cylindrical surface. Recessed features are ground near ends of an equatorial diameter to form obtuse edges, kinematically defining the departure height of the suspension wire, with some axial adjustment allowed for balancing (see Figure 1). The plane of these edges is placed above the center of mass of the body such that the “pitch” normal mode eigenfrequency is approximately 1 Hz (since the body will be wedged, the edges may still lie on a geometric diameter). A shallow V-groove around the equator of the testmass retains the wire for safety.

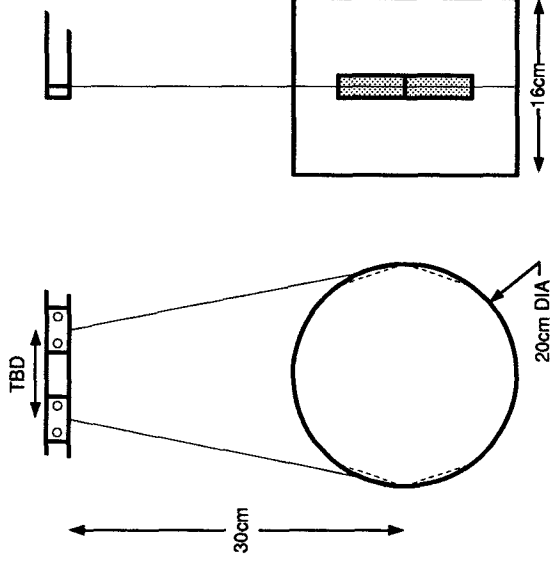


Figure 1: Schematic of testmass with conceptual detail of kinematic wire departure.

To meet LIGO initial receiver requirements, the total thermal noise contribution of internal modes of each test mass cannot exceed 1.4×10^{-20} m/ $\sqrt{\text{Hz}}$ at 100 Hz. Depending on the exact nature of the damping and the resulting Nyquist force power spectrum, this can be translated into a range of equivalent Q 's for the internal modes of the test masses. For two particular models, viscous damping ($Q \propto 1/f$) and internal damping (Q independent of f), the first three effective normal modes of the cylinder are required to have $Q_{\text{visc}} \gtrsim 10^4$ or $Q_{\text{int}} \gtrsim 10^6$ respectively [2, 3].

2.2 Suspension

The mass hangs in a single loop of hard drawn steel wire (“piano wire”), of diameter such that it is loaded to one half the breaking stress (roughly 300 μm diameter). The upper ends of this wire are clamped by fixtures to a rigid plate, which forms the upper

end of a boxlike *cage* (Figure 2). The wire length places the center of mass of the test mass 30 cm below the wire clamping points.

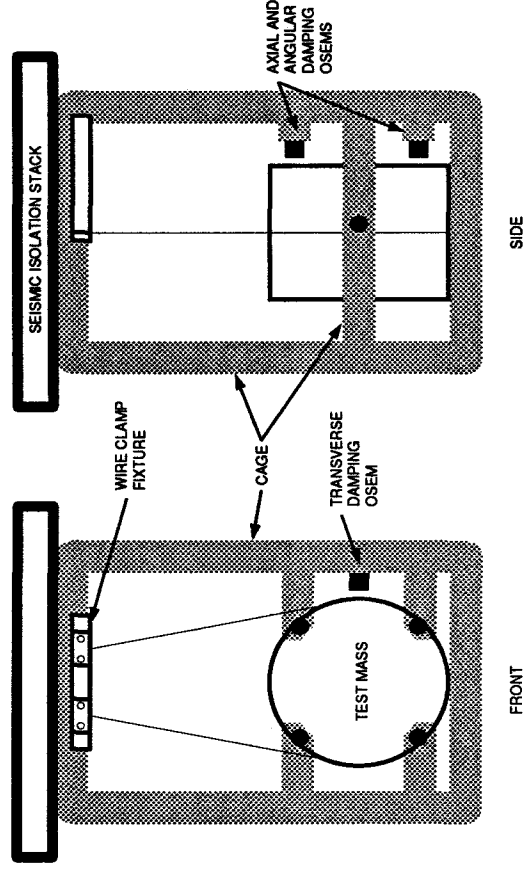


Figure 2: Testmass suspension cage concept, showing OSEM controller mounting locations. Mechanical protection limit stops are omitted for clarity.

The cage surrounds the suspended mass and provides mounting provision for local sensors and force actuators, as well as mechanical limit stops for earthquake protection and handling. The cage itself is mounted (via either its upper or lower surface) to the termination of the Seismic Isolation Stack.

The wires attachments are horizontally spaced such that the “yaw” normal mode has an eigenfrequency of 1 Hz.

The target strain spectrum assumes that thermal noise in the pendulum suspension limits interferometer performance between about 40 and 140 Hz. This limit is based upon assuming a viscous damping mechanism and a Q of 10^7 (measured at the 1 Hz eigenfrequency). If the true damping mechanism is not viscous but so-called internal damping [2], significantly lower Q at 1 Hz could correspond to the same 100 Hz noise level. In computing the effects of eddy-current damping on the test mass (a viscous process, see §D.3) we have required the Q to remain at least 10^7 .

2.3 Sensors and actuators

Integrated local sensors and magnetic force motors, similar to the OSEM systems now in use [14] but with improved outgassing properties and possibly with reduced noise level, are mounted to the cage. Four OSEMS interact with rare earth permanent magnets and shadow masks at four places around the periphery of the back of the

mass. These four magnets are poled such that the assembly has no net dipole moment. They are bonded directly to the surface of the mass using low-dissipation epoxy, and the shadow masks are similarly bonded to the magnets. Another OSEM senses and controls transverse horizontal motion, its magnet and vane attached radially near the equator. An additional magnet is bonded opposite, again to cancel the net magnetic dipole moment. A similar arrangement can be provided for vertical damping as required (a satisfactory method of increasing the vertical compliance is TBD).

The permanent magnets each have a magnetic dipole moment $\mu \approx 3 \text{ mA m}^2$, roughly a 1.5 mm diameter by 2.2 mm length cylinder of standard magnetic material¹. This is one tenth the dipole moment of the OSEM magnets currently in prototype service.

2.4 Control systems

Of the six rigid-body degrees of freedom of the test mass, four may be locally damped by the OSEM system and two, vertical translation and rotation about the optic axis, are constrained by the wires². Residual noise from the local sensors must be filtered away with a high rate of rolloff between the frequency of the required damping (of order one to two Hz) and the signal band (100 Hz for the initial LIGO receivers). This rolloff rate is constrained by control system stability requirements.

A hierarchical control topology, analogous to the "local/global" orientation loop hierarchy in the 40m prototype, is used to partially circumvent this difficulty (Figure 3). The sensor function of each controlled degree of freedom can be "handed off" from the local sensor to a global sensor of higher accuracy and lower noise (but possibly with lesser dynamic reserve or robustness) after startup. For example, the local OSEM signals provide pitch and yaw damping and D.C. error signals which align the test mass coarsely, perhaps to $\sim 5\mu\text{rad DC}$ accuracy and with $\sim 10^{-9}\text{rad}/\sqrt{\text{Hz}}$ equivalent noise. After coarse alignment is achieved, optical levers and/or optical phase gradient sensor are switched into the loop and the local sensors are ignored. Similarly, axial translation control is handed off to optical phase error signals originated by the Interferometer and Cavity systems.

In the current design, only the transverse motion lacks an alternate sensor of higher quality. Its OSEM sensor noise is thus impressed on the test mass, and will induce excess strain noise if its force axis is not perfectly orthogonal to the optic axis and if its residual noise not filtered successfully out of the signal band. A viable control system loop transfer function with sufficient filtering for initial LIGO goals, assuming prototype OSEM noise and a 5% cross coupling from transverse to axial motion, is shown in Figure 4. Briefly, the compensator stabilizes the 1 Hz pendulum with a pair of real zeros at 0.1 Hz, and rolls off with a complex pole cluster comprising a 9th order Butterworth lowpass filter at a corner frequency of 8 Hz and a 2nd order Butterworth at 4 Hz. This combination, along with the 1 Hz pendulum response, has an attenuation of 6×10^{-14} at 100 Hz when set to have unity gain at 1.2 Hz, and falls as f^{-11} asymptotically. At this gain the closed-loop response peaks out at about 8 dB

¹Electron Energy Corporation's Remco-18, for example.

²In the sense that the wire tension restoring force drives the frequencies of the corresponding eigenmodes to well above 1 Hz.

near the 1 Hz pendulum frequency and the step input settling time is approximately three seconds. While this is a viable loop transfer function, it is by no means optimal, and further study may yield considerable improvements in damping, settling time and stopband attenuation.

3 Departures from direct prototype scaling

The proposed design differs in several details from the 40m prototype. Some justifications for these differences follow.

3.1 Monolithic mirror/mass

We plan to use monolithic mirrors in the 40m as soon as practical; the Glasgow, ISAS (Tokyo) [6] and Garching [5] prototypes do so already. One possible advantage of optically contacted mirrors could be that the substrate optical transmission difficulties are minimized by reducing substrate thickness, but substrate effects are currently thought to be insignificant at initial LIGO receiver performance levels [4].

3.2 Single loop suspension

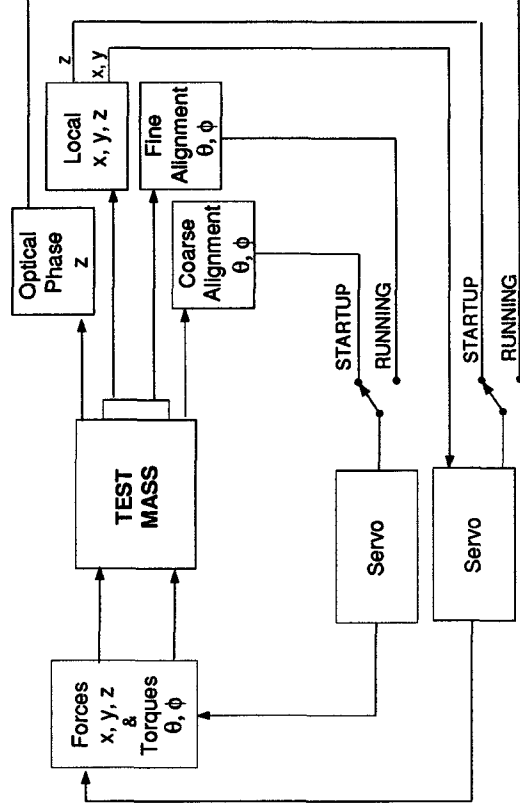
The single loop suspension is more readily compatible with the control actuator system we have chosen (see §3.4). While we don't currently hang the 40m test masses with single loop suspensions, we do use such a system on the beamsplitter. The Garching and the ISAS interferometers have used single loop suspensions successfully.

3.3 Reference/mounting for sensors and actuators

Sensors and actuators on the 40m prototype are sprinkled around liberally between seismically isolated, semi-isolated, and noisy platforms. The main (axial) drive coils are mounted (effectively) to the ground, as are the axial damping sensors (the "shark detectors") for the end masses. The damping feedback actuators (wire pushers), however, are mounted on the seismic isolation stacks, as are the angular control torque actuator coils. For the vertex masses and the beamsplitter a second (lower) stack with only two layers moderately isolates the shark sensors and OSEMs.

Seismic noise would compromise the isolation by feeding into the test mass through the damping system if the OSEMs were referred to ground; also, if the OSEM actuator coils were decentered or misplaced with respect to their magnets, a force gradient would develop which would multiply coil motion by any DC or low-frequency feedback force. These problems practically preclude mounting the local control sensors and actuators to the ground (see §D.2).

Drift of the seismic isolation stack and possibly enhanced RMS motion at the resonant frequencies of the stack may pose complications. Current designs call for the stack to be periodically leveled, and for its Q to be low as well [8].



LS/MEZ
9/12/91

Figure 3: Test mass control topology, showing handoff between robust "local" control sensors in startup mode and "global" sensors (of higher accuracy and lower noise) for normal operation.

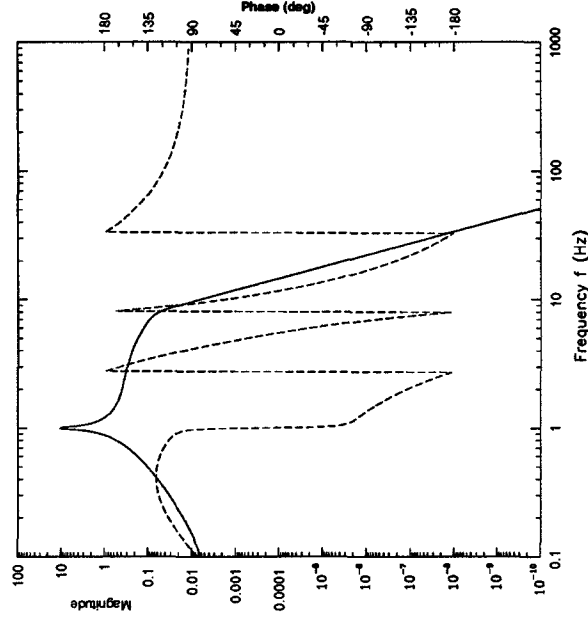


Figure 4: Bode plot of a control loop design which avoids interference of OSEM noise in the transverse test mass damping loop with initial LIGO receiver strain performance goals. Noiseless drive circuits are assumed. See text for other conditions.

3.4 Direct magnetic drive for all degrees of freedom

As in the previous category, this is not so much a departure as a choice from the variety of techniques used on the 40m. The Garching and ISAS detectors use direct magnetic drive for all degrees of freedom, while the 40m prototype employs direct drive for axial force and indirect magnetic drive for torques (i.e. torques are applied through a torsionally rigid arrangement of suspension wires by way of a "control block" at the suspension point, see Appendix A). Gain and bandwidth constraints virtually demand direct drive of the mass at some level (the finite propagation speed of corrections applied via the suspension wires limits bandwidths to the order of 100 Hz). There is a potential benefit in reducing the coupling strength by up to a factor of 100 by augmenting a weakly coupled (thus potentially lower noise) direct drive with some low-bandwidth wide range indirect drive, at the expense of complication, but this has not been quantified.

3.5 Low bandwidth damping and control loops

The installation of angular orientation systems with characteristic Bode plots like Figure 4 is almost complete in the 40m system, so this is technically less a departure than an update. The shark detector damping system was also modified to achieve similar goals. Both systems now give improved prototype performance.

4 Risks and open questions

In this section we highlight some problems for which current models and existing prototype experience are deemed insufficient to confidently project performance or practicality. This is intended to serve as focus for motivating future experimental and/or theoretical investigation.

4.1 Thermal noise

There is currently no reliable basis on which to predict the thermal noise contributions from modes of the apparatus. In this sense thermal noise constitutes a major risk.

4.1.1 Internal test mass modes

Measurements of the Q 's of internal modes of actual test-mass-like objects have mostly been at high frequencies, the normal mode eigenfrequencies typically ranging in the tens of kHz. Predicting the thermal noise contribution two decades lower in frequency from such a measurement requires faith in some physical damping mechanism. Measurements of modes on some systems seem to suggest viscous damping [7] while others imply internal damping [18] and others fit neither³.

³For example the test masses in the 40m prototype at this writing have Q 's between 2,000 and 20,000 for different modes, with no obvious pattern of dependence on eigenfrequency.

4.1.2 Pendulum mode

As with internal modes, the pendulum thermal noise can't yet be predicted with confidence. The proposed target spectrum was assumed to be limited by thermal noise over a substantial frequency band, from 40 to 140 Hz. The Q of 10^7 chosen for that model was based upon measurements of a specially prepared pendulum in Glasgow [11], and the damping mechanism was assumed to be viscous since in this regime that produces a more conservative limit. Some of us expect the damping to be "internal," i.e. produce less noise above the resonant frequency, but then again, many of us are concerned that $Q \sim 10^7$ may be difficult to achieve in practice.

4.1.3 Vertical wire extension mode

The pendulum Q is substantially greater than the the intrinsic bulk Q of the wire material, since in the pendulum oscillation at least 10^4 times as much energy is stored in the gravitational field as in the bending of the wire material. This factor is absent for the vertical "bobbing" eigenmode of the mass; what's more, this mode will lie at 10 Hz or so if no spring or other compliance is introduced. The slope of the interferometer beam with respect to the local gravitational equipotential will be on the order of three parts in 10^3 , so if the vertical thermally-agitated displacement exceeds the horizontal by a factor of 300 or more, its contribution to the interferometer strain noise will be greater.

4.2 Magnet-related noise

Experience with suspended prototypes leads to the conclusion that for the near future, the surest way to control test mass motion with sufficient bandwidth and strength is by interacting with permanent magnets attached to them. Until an electrostatic or other drive system can be demonstrated, we are stuck with having some number of magnets, of greater or lesser size, attached. This brings to mind a series of possible noise and interference risks.

4.2.1 Lightning storms

In §D.6 we show that lightning can conceivably provide correlated signals over fairly wide baselines. A very simple magnetic event veto system and/or modest magnetic shielding can be used to eliminate these events. More data are required on the actual occurrence rate, strength, and attenuation of these pulses for actual site locations.

4.2.2 Barkhausen effect

The flipping of magnetic domains in the magnet material, triggered thermally or by imposed low-frequency fields, could lead to high frequency noise. Experiments are being devised to look for this effect by monitoring the magnetization in rare-earth magnets.

4.2.3 Glue joint noise

Experiments done on the Glasgow 10m prototype interferometer seem to show that glue joints between mirrors and test masses induce noise [16]. There is a further suspicion that applying large low-frequency forces to magnets will induce high-frequency noise in the glue that bonds them to the test mass. The mechanism of noise generation, the spectral form of the noise, and the dependence on glue properties, area and thickness are not known. Further experiments are needed to see if upconversion is a serious problem.

4.2.4 Eddy current Q degradation or seismic "short"

Eddy currents will cause viscous coupling of a test mass having small residual dipole and quadrupole moments to the vacuum vessel or to metallic suspension parts nearby. For the suspension parts mounted to the seismic isolation stack, the only requirement is that the damping not wreck the Q of the suspension; for the vacuum chamber, however, damping at a much lower level will couple seismic and acoustic noise directly to the mass, short-circuiting the isolation stack and pendulum.

4.3 Control system driver output noise

We have assumed that control systems are limited entirely by the SNR of the sensors which provide their error signals. It is possible that the transfer function in Figure 4 will be very difficult to implement without a significant contribution of electronic noise from the servo compensation electronics. A focused practical design exercise, taking account of the trade between dynamic reserve, gain and SNR, should be undertaken to find out whether such "output noise" contributions can be limited to the required level. Alternate suspension designs (e.g. double pendula) may require more complicated compensation but could in principle improve the tradeoff between input and output noise, by replacing electronic poles with potentially quieter mechanical poles. Whether this can be realized in practice depends crucially on what component really is the limiting factor; indeed, in our simplified "front-end-dominated" noise models, all systems with the same loop gain have identical residual noise, irrespective of whether poles are implemented mechanically or electrically.

APPENDICES

A Alternate suspension arrangements

The 40m interferometer uses an intermediate control block to transmit torsional and low-bandwidth axial feedback forces down to the test mass through the suspension wires. The block is constrained in translations and in roll, but is relatively free to rotate about the pitch and yaw axes. Two loops of wire clamped to the block support the mass below.

The mechanical transfer function of this system has been measured and is poorly understood at this time. Its isolation appears to be considerably worse [15] than is expected (and has been measured, see [5]) for a single loop clamped rigidly to the supporting structure.

A.1 Double pendulum

A more promising variant, as yet untested in a prototype, is a "double pendulum." An intermediate mass is used, but it is left unconstrained in translations as well. Potential benefits include improved seismic isolation (especially if the intermediate mass is roughly the size of the test mass) and relaxed filtering and output noise requirements for some subset of the control system drivers, since some filtering can now be shared by additional mechanical poles. In addition, the peak force applied directly to the test mass can be reduced by a factor of 30 to 100, by introducing the lowest-frequency (largest) corrections at the intermediate mass instead. This can reduce any nonlinear noise generation at the magnet glue joints and allow use of smaller magnets (or electrostatic drive) to reduce the effect of environmental fields. Possible pitfalls include the higher complication of construction and control system compensation, which must cope with additional resonances (that is, the additional poles are undamped) and also additional degrees of freedom. Advanced interferometers may require the additional seismic isolation of a double pendulum.

A.2 Multiwire single pendulum

If there is difficulty in balancing the mass in a single loop sufficiently well that D.C. pitch torques are not excessive, two wire loops arranged very close to each other could be used. The loop lengths would be adjusted to establish the equilibrium pitch of the mass at D.C., and their axial separation, along with the height of the wire departure edges, would be arranged to give the desired pitch mode eigenfrequency. This concept could be extended to several wires if there is a finding that sharing the load among multiple wires improves thermal noise or some other property.

B Control system sensor noise

Interferometric servo controls which are applied with high bandwidths ($\gtrsim 20$ Hz) are likely to be challenging design problems because of internal resonances in the test mass. For damping systems, however, the main objectives are to efficiently minimize the RMS motion at the eigenfrequencies of the mass suspension without introducing excess noise, from the environment or the sensors, at higher frequencies.

The strategy of shutting off direct control of axial position by local sensors as soon as the relevant interferometer signal is acquired leaves only the transverse and vertical translational degrees of freedom active during operation. These, and the angular degrees of freedom, must be damped by a control system which is stable and yet attenuated enough at 100 Hz not to introduce excess strain noise.

B.1 Coupling to transverse or vertical damping

Seismic noise transmitted through the stack, shaking the OSEM sensor itself, will cause excess apparent displacement noise; however, as long as the control system transfer function falls at least as rapidly as the pendulum transfer function between 1 Hz and 100 Hz (i.e. $1/f^2$ or faster) this transmission path will not exceed direct mechanical transmission. We only consider control systems with this property.

Current OSEMs deliver shot noise-limited performance corresponding to a white displacement spectral density $\dot{z}_O(f) \lesssim 10^{-10}$ m/ $\sqrt{\text{Hz}}$ over a broad range of frequencies between 5 Hz and 5 kHz (Table 1). This appears to be the dominant "source" for excess translation noise.

As mentioned, the transverse and vertical damping⁴ are the only loops still referred to the local sensor when the interferometer is making observations. These damping systems will in principle not afflict the cavity axis, but we anticipate that because of mechanical misalignments, assembly tolerances, and nonuniformity of magnets the control forces will develop a component which perturbs the mass axially. We characterize this component by an angle $\zeta = F_{\text{axial}}/F_{\text{transverse}}$. Based on considerations of assembly tolerance and field uniformity we estimate $.001 \lesssim \zeta \lesssim .05$, that is, the spurious axial component is between .1% and 5% of the total force. The resulting axial displacement of each mass is then

$$\begin{aligned} \ddot{z}(f) &\gtrsim \zeta \dot{z}_O(f) \times \frac{\mathbf{H}(f)}{1 + \mathbf{H}(f)} \\ &\gtrsim \zeta \dot{z}_O(f) \times \mathbf{H}(f) \end{aligned} \quad (1)$$

since $\mathbf{H}(f)$, the forward loop transfer function including electronic and mechanical features, is quite small at frequencies of observational interest. Using the transfer function \mathbf{H} shown in Figure 4 and the measured OSEM noise (Table 1) we predict the noise contribution from each test mass of the interferometer; multiplying by $\sqrt{4}$ and dividing by $L = 4$ km gives the predicted contribution to the interferometer strain spectrum shown in Figure 5.

⁴If vertical damping is employed.

It is unclear whether damping is required for the vertical mode of the suspension, since its frequency may be high enough that we can tolerate its RMS excitation. If vertical damping is employed the control system must be frequency-scaled to the appropriate eigenfrequency, perhaps 10 Hz. Translating the predicted control system noise contribution shown in Figure 5 a decade up in frequency will violate the initial interferometer sensitivity goal (see §D.3). We have concluded that it would be difficult to damp this mode quietly enough unless either a much quieter sensor is used (say a modest laser interferometer, about a thousand times quieter) or vertical compliance is added to the suspension to bring its vertical eigenfrequency down to about 1 Hz. We expect future work on suspension thermal noise to have a significant impact on the vertical eigenfrequency problem.

B.2 Coupling to optical lever noise

For angular control we have used an optical lever system as a model with which to test the suitability of the control concept. We presume that an automated alignment system will have equal or lower noise to this system, which we have sparsely outlined in Appendix C. Under conditions we believe are readily achievable, the white shot-noise limited angle spectral density of this sensor should be $\tilde{\theta}(f) \approx 10^{-11}$ rad/ $\sqrt{\text{Hz}}$ over a broad range of frequencies.

This angle sensor noise, transmitted through the control system, can induce spurious changes in apparent arm length by two principal mechanisms. First, the angular signal may be processed imperfectly, such that the feedback forces are not applied to the test mass as perfect couples and there is a net force in addition to the desired torque. Second, the optical cavity axis may be displaced with respect to the principal inertial axes of the test mass. At frequencies well above the rotational eigenfrequencies of the suspension, the mass will rotate about these principal axes in response to applied torques. If the optical cavity axis is displaced laterally by an amount d the apparent change in cavity length will be $\delta z \approx d \delta \theta$ for an angle change $\delta \theta$ [17].

We apply the angular control torque τ with approximately equal and opposite forces $F_i = \tau/2R$ at opposite edges of the test mass (radius R). Failure to balance the forces by a fractional error ξ leaves a net force on the mass

$$\xi F_i = M \ddot{z} = \xi \frac{l \ddot{\theta}}{2R}, \quad (2)$$

or

$$\frac{\ddot{z}}{\ddot{\theta}} = \frac{z}{\theta} \approx \xi \frac{l}{2MR}.$$

The moment of inertia of a cylinder of radius R and length l about axes perpendicular to its symmetry axis is

$$\frac{I_x}{M} = \frac{I_y}{M} = \frac{R^2}{4} + \frac{l^2}{12} \approx 4.6 \times 10^{-3} \text{ m}^2 \quad (3)$$

for the shape we described in §2.1, so we can expect a spurious displacement due to control system angle noise of

$$\ddot{z}(f) \gtrsim \xi \frac{l}{2MR} \mathbf{H}(f) \tilde{\theta}(f)$$

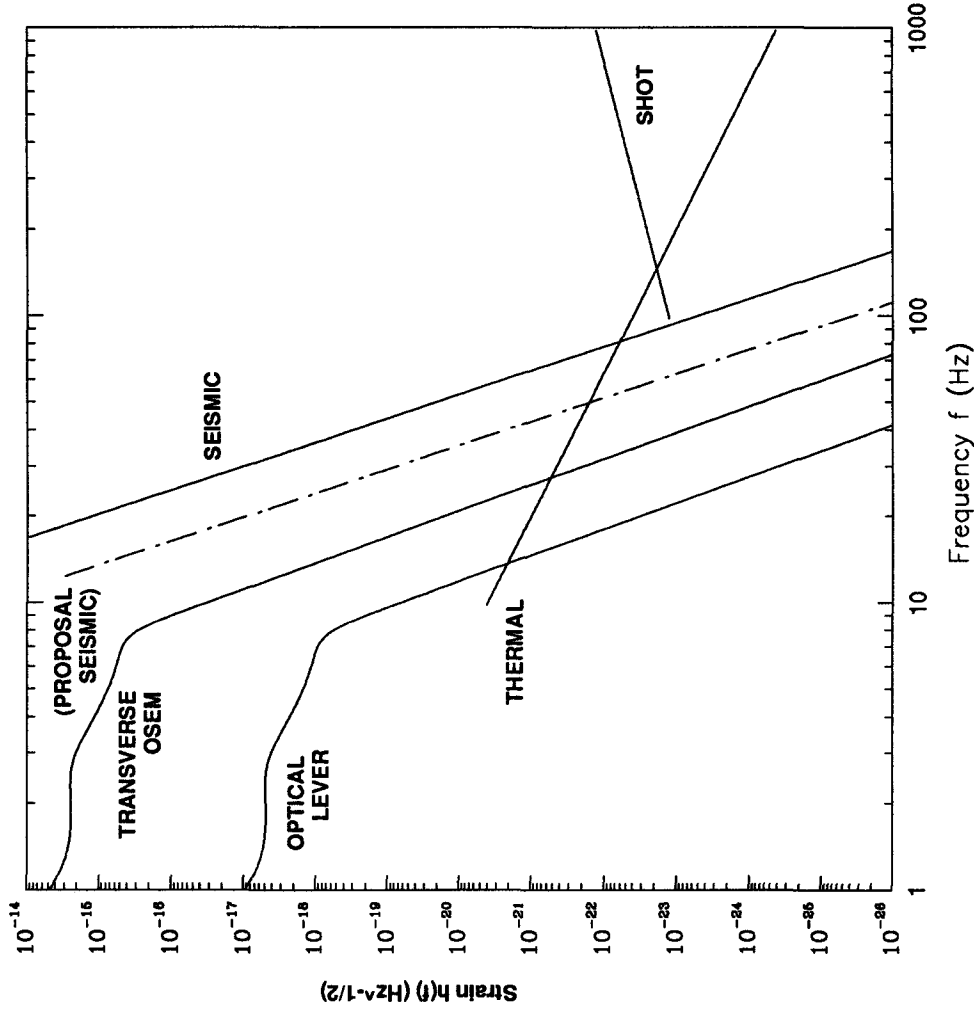


Figure 5: Predicted strain contributions due to residual test mass control system sensor noise. Noise from OSEM transverse damping sensors and from a simple optical lever angle sensor (§C), filtered by the forward transfer function shown in Figure 4, is summed in quadrature for all relevant degrees of freedom of each of the four test masses. Transverse translation noise is assumed to be introduced by a force vector misalignment $\zeta \approx 5\%$. Orientation noise coupling is modeled by a static beam axis—inertial axis offset $d \approx 1\text{mm}$. Also shown are calculated interferometer shot noise, thermal noise and seismic noise from Figure V-3 of [10], and a newer seismic noise estimate based on modelling of the stack under construction at MIT [13].

$$\approx 4 \times 10^{-5} \mathbf{H}(f) \tilde{\theta}(f) \frac{\text{m}}{\text{rad}} \quad (4)$$

for an imbalance $\xi = 1\%$ ⁵. Inserting the generic control loop transfer function $\mathbf{H}(f)$ (Figure 4) for the angle control loop and the derived optical lever sensor noise $\tilde{\theta}(f) \approx 10^{-11} \text{ rad}/\sqrt{\text{Hz}}$ we obtain a predicted displacement contribution of $1.2 \times 10^{-23} \text{ m}/\sqrt{\text{Hz}}$ (per mass, per degree of freedom) at 100 Hz. The quadrature sum for all eight angular control systems is well below the initial interferometer target spectrum.

If the optical cavity axis is decentered from the inertial axis of the test mass by “impact parameter” d , rotational control signals will directly induce displacement of the “average” mass position sensed by the beam. The noise introduced by this simple lever-arm mechanism is

$$\tilde{z}(f) \gtrsim d \cdot \mathbf{H}(f) \tilde{\theta}(f). \quad (5)$$

For a plausible beam offset of 1 mm (in both x and y directions), and taking once again the generic transfer function $\mathbf{H}(f)$ and optical lever sensor noise $\tilde{\theta}(f)$, we estimate a test mass displacement of $4 \times 10^{-23} \text{ m}/\sqrt{\text{Hz}}$ (per mass, per degree of freedom) at 100 Hz. The predicted impact on the interferometer strain spectrum is shown in Figure 5.

C Optical lever concept and noise estimate

The sensor noise assumed in §B.2 is derived from a simple model of an optical lever alignment system. While the design of the alignment system is beyond the scope of this work, we make the assumption that the chosen system will perform no worse than this crude model.

We imagine using the scheme presented by Ron Drever in which a “pilot beam” is transported the length of the enlarged vacuum “manifold” in each station (about 40m or so total length). The originating laser/telescope system and a position-sensitive detector (quadrant diode) are placed on geometrically stable foundations, perhaps outside the vacuum system, at extreme ends of this manifold. The pilot beam is servo stabilized in direction to remain centered on the quadrant diode, fixing the beam’s orientation with respect to the stable foundation members.

Light is “dipped” out of this pilot beam by a partially transmitting periscope and fed to a shallow-angle prism, held at minimum-deviation incidence. The diverted beam direction will be largely insensitive to motion of these optical components. Their combined action directs the beam to the coated surface of the test mass.

The reflection from the test mass is directed onto a quadrant photodetector a distance D away, possibly by a similar optical system used in reverse; the beam arrives here having radius w ⁶. Lenses may be needed to transform the diameter to a practical detector size if necessary, but for calculation purposes we may assume a sufficiently large detector. The four photocurrents are processed to yield mirror angle errors θ and ϕ .

⁵In principle we could experimentally trim ξ to zero with very high accuracy, perhaps to a part in 10^6 , but we do not rely on doing this.

⁶Optical apertures are sufficient, and D is small enough, that the far-field diffraction approximation $w \propto D$ is not appropriate. For aperture radius $a \sim 5\text{cm}$, we can get $w \gtrsim 2D\lambda/a \sim 1 \text{ mm}$.